



HAL
open science

Marangoni destabilization of bidimensional-confined gas-liquid co-flowing streams in rectangular microfluidic channels

M. Clerget, A Klimenko, M. Bourrel, F. Lequeux, P. Panizza

► **To cite this version:**

M. Clerget, A Klimenko, M. Bourrel, F. Lequeux, P. Panizza. Marangoni destabilization of bidimensional-confined gas-liquid co-flowing streams in rectangular microfluidic channels. *Physics of Fluids*, 2023, 35 (4), pp.042111. 10.1063/5.0145178 . hal-04089814

HAL Id: hal-04089814

<https://hal.science/hal-04089814>

Submitted on 9 May 2023

HAL is a multi-disciplinary open access archive for the deposit and dissemination of scientific research documents, whether they are published or not. The documents may come from teaching and research institutions in France or abroad, or from public or private research centers.

L'archive ouverte pluridisciplinaire **HAL**, est destinée au dépôt et à la diffusion de documents scientifiques de niveau recherche, publiés ou non, émanant des établissements d'enseignement et de recherche français ou étrangers, des laboratoires publics ou privés.

Marangoni destabilization of bidimensional-confined gas-liquid co-flowing streams in rectangular microfluidic channels

M. Clerget,^{1,2} Alexandra Klimenko,² Maurice Bourrel,² François Lequeux,³ and Pascal Panizza^{*3,4}

¹Laboratoire Physico-Chimie des Interfaces Complexes, Bâtiment CHEMSTARTUP, RD 817, 64170 Lacq, France

²TotalEnergies S.E., Pôle d'Etudes et de Recherches de Lacq, BP 47, 64170 Lacq, France

³Laboratoire Sciences et Ingénierie de la Matière Molle, ESPCI Paris, PSL University, Sorbonne Université, CNRS UMR 7615, 75005 Paris, France

⁴IPR, UMR CNRS 6251, Campus Beaulieu, Université Rennes 1, 35042 Rennes, France

(*corresponding author : pascal.panizza@univ-rennes1.fr)

(Dated: 9 May 2023)

In microchannels, the stability of a fluid jet injected into another immiscible fluid strongly depends on its degree of geometric confinement. When the width of the jet, w , is larger than the channel height, H , the surface tension driven Rayleigh-Plateau instability is suppressed so that the 2D (bidimensional)-confined jet is absolutely stable and never collapses into bubbles (or drops) in contrast to what occurs when $w \leq H$ ^{1,2}. We here demonstrate both experimentally and theoretically, that this picture is indeed no longer valid when Marangoni effects are considered. We experimentally show that the addition of small length alcohol molecules into the liquid phase destabilizes a 2D-confined gas-water microfluidic stream ($w > H$) leading to the generation of steady non-linear waves and further to the production of bubbles. Using a simple hydrodynamic model, we show through a linear analysis that the destabilization of the gas stream may result from a Marangoni instability due the fast adsorption of the alcohol molecules which occurs on a time scale comparable to that of the microfluidic flow.

I. INTRODUCTION:

The breakup of a cylindrical unconfined fluid jet injected into another immiscible fluid is a natural phenomenon that each of us witnesses daily when having a shower, drinking at a water fountain or blowing soap bubbles³, for instance. This phenomenon which has to be either controlled or avoided in many industrial and technological applications including polymer extrusion⁴, spray atomization^{5,6}, ink jet printing^{7,8}, emulsification^{9,10} or foam generation¹¹, has been a major topic of research in hydrodynamics and soft matter for more than two centuries¹². Since the seminal works of Plateau and Rayleigh^{13,14}, it is acknowledged that quiescent fluid cylinders are unstable and break-up into drops or bubbles as a result of the surface tension driven Rayleigh-Plateau instability. However, the effect of geometric confinement on the stability of co-flowing systems made of two immiscible fluids may drastically change this picture^{1,2,15}. Confined co-flows have drawn great interest over the last two decades^{16–22} because of their relevance for the microfluidic production of highly monodisperse droplets^{23–26} or bubbles.^{27–31} Two standard microfluidic methods to produce monodisperse droplets or bubbles are the cross-flow geometry which consists of an intersection of a main channel with two symmetrical side ones and the axisymmetric flow focusing geometry where a needle is centred into a capillary tube. By injecting the dispersed liquid (or gas) through either the main channel or the needle and the outer fluid through either the side channels or the outer gap between the needle and the tube, one obtains of central liquid (or gas) stream that is stable or breaks up into monodisperse droplets, depending on the operating conditions (e.g. flow conditions, physico-chemical parameters of the fluid and geometrical parameters of the device). Since the pioneering works of and Cramer *et al.*³² and Anna *et al.*²³, a tremendous

amount of works^{33–38} has been devoted to the study of the influence of these operating parameters on the jet/droplet (or bubble) transition, as well as on the size of the droplets produced or the width of the stable jets that are formed. The existence of two regimes of breakup: dripping in which droplet pinch off near the location where the two immiscible fluids meet (respectively the cross flow junction or the tip of the needle) and jetting in which the droplet pinch off from an extended thread downstream have been identified^{17,18}. Using a lubrication approximation and neglecting inertial terms, Guillot *et al.*¹⁷ have performed a linear stability analysis on the developed flow profile for an axisymmetric jet and shown that the transition from dripping to jetting is related to an absolute convective transition of the Rayleigh plateau instability, a conclusion that was also reached by Utada *et al.*¹⁹. Using this approach and neglecting the angular dependence of the perturbations, they have also numerically investigated the case of a co-flowing jet confined in a rectangular conduct that is the most encountered geometry in microfluidic experiments and shown that the stability of such a jet strongly depends on its degree of geometric confinement. When the width of the inner thread, w , is larger than the channel height, H , the surface tension driven Rayleigh-Plateau instability is suppressed so that the 2D-confined jet is absolutely stable and never collapses into drops or bubbles in contrast to what occurs when $w \leq H$ ^{1,2}. This theoretical prediction has been experimentally checked by Humphry *et al.*¹⁵ and de Saint Vincent *et al.*³⁹ for liquid/liquid coflows as well as by Dollet *et al.*¹ for non-wetting gas 2D-confined streams. It has also been theoretically confirmed by Cabezas *et al.*²⁰ using a more refined hydrodynamic theoretical model.

In this article, we investigate the effect of surface active molecules on the stability of a 2D-confined gas-liquid jet. We show that the behaviour of the jet changes drastically when

small length alcohol molecules are added into the liquid phase leading to its destabilization and to the formation of steady non-linear waves, although the jet is $2D$ -confined and should therefore be stable. Using a simple hydrodynamic model, we show through a linear stability analysis that this red new reported phenomenon may result from a Marangoni instability due to the fast adsorption of the alcohol molecules onto the gas-water interface as it occurs on a timescale comparable to that of the microfluidic flow.

II. EXPERIMENTAL SECTION:

A. Materials

In our experiments, we work with mixtures of butan-1-ol (Sigma Aldrich) and deionized water containing 1 g/L of NaCl (Sigma Aldrich). In order to ensure the wettability of the microfluidic channels, we have added 1 wt % of Tween 20 (Fisher Scientific). In our study, x_{but} , the mass fraction of butanol is either 0 or 7 %. The water/butan-1-ol solution is first prepared and then mixed with Tween 20 and stirred to obtain an homogeneous mixture. All our experiments are performed at $T=23^\circ\text{C}$. The viscosities of the system with and without butanol measured with a Rheometer *Low shear* 400 from Lamy rheology are respectively 1.1 and 0.96 mPa.s. The values of the equilibrium surface tension of these liquid solution with N_2 are respectively 33.6 and 25.4 mN.m⁻¹ for the system without and with butanol. These values are determined with a tensiometer (*TrackerTM* from Teclis Scientific, France) that measures the shape of rising N_2 bubbles formed in the liquid solutions⁴⁰. The time to reach the equilibrium value surface tension value is very short for the butanol system (less than 1s the resolution of this apparatus) whereas it takes several minutes for the system without butanol. Using a commercial maximum bubble pressure tensiometer, *BPA2S* (SINTERFACE Technologies, Germany), we characterize the dynamic surface tension of the solutions at much shorter times. This apparatus⁴¹ permits to estimate very short adsorption times from dynamic surface tension data acquired in a bubble lifetime t_{life} interval from 10^{-2} s up to 10 s, and even down to $t_{life} = 10^{-3}$ s for solutions with water as solvent^{42,43}. In Fig. 1, we observe that the adsorption of butanol molecules onto the gas/liquid interface is much faster than that of the Tween 20 surfactant molecules. At $t_{life} = 10^{-2}$ s, the value of the surface tension for gas/solution with butanol system is roughly the equilibrium one indicating that the adsorption of the butanol molecules on the gas interface at this timescale is already total. In contrast, at $t_{life} = 10^{-2}$ s, the value of the surface tension for the gas/solution without butanol system, which has not relaxed yet to its equilibrium value, is still large indicating that the adsorption process of Tween 20 surfactant molecules onto the gas interface is red much slower. From additional experiments conducted at $t_{life} \simeq 10^{-3}$ s on the Tween 20 surfactant solution with no butanol, we deduce that Tween 20 surfactant molecules do barely not absorb on the gas/liquid interface at on the millisecond time scale since the value of the measured surface tension remains close to that of water

$$\gamma_w = 72.4 \text{ mN.m}^{-1}.$$

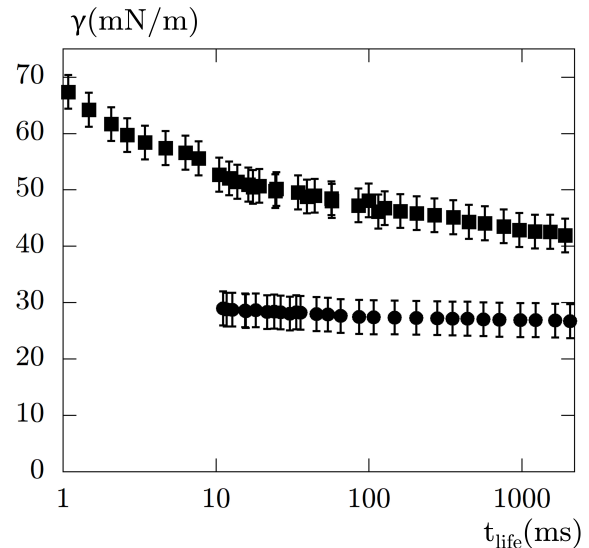


FIG. 1. Dynamic surface tensions measured for the surfactant solution made of 1 wt % of Tween 20 with 0 wt % (■) and 7 wt % (●) butanol over the interval 1 ms – 2000 ms using the maximum bubble pressure method. Values under 10 ms for the 7 wt % butanol solution cannot be obtained due to technical limitations of the apparatus^{42,43}.

B. Microfluidic experiments

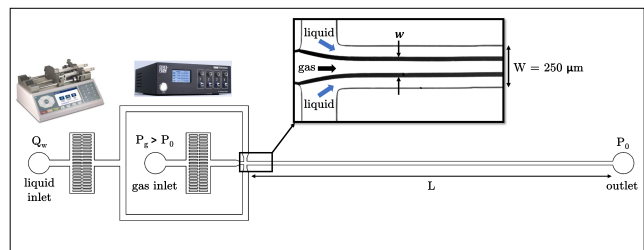


FIG. 2. Top view sketch of the set-up and definition of the geometric parameters characterizing the channel and the gas jet. Insets : images of the syringe pump (Nexus 3000 from Chemyx, USA) and the gas pressure controller (OB1 MK3+ from Elvexsys, France) used to conduct our experiments. Inset: image of the inner gas stream that forms at the cross junction where gas and liquid meet.

Our microfluidic experiments are carried out in planar microchannels, fabricated by soft lithography techniques⁴⁴: a molding of poly(dimethylsiloxane), PDMS (Sylgard 184 Silicone Elastomer, Dow Corning) is sealed to a smooth PDMS slab using a plasma treatment, which also makes the channel surfaces hydrophilic. Laminar gas-liquid co-flowing streams are formed at a symmetrical cross flow junction (see inset of Fig. 2). The inner dimensions of the main channel are $H=63 \mu\text{m}$, $W=250 \mu\text{m}$ and $L=2.4 \text{ cm}$. The gas (N_2) is introduced through the central channel and the liquid from the two lateral channels, respectively, as depicted in Fig. 2. The liquid

flow rate, Q_w , is controlled by a syringe pump *Nexus 3000* (Chemyx, USA) whereas N_2 is delivered through the gas inlet from a pressurized tank (pressure $P_0 + \Delta P$) by means of a pressure controller *OB1 MK3+* (Elvesys, France). The main channel outlet is at atmospheric pressure, P_0 . The set-up is placed under an inverted microscope *DM IL LED* (Leica, Germany) with a 5–10 x objective, which is connected to a high-speed camera *FASTCAM Mini AX100* (Photron, Japan). The rate of acquisition is 20000 frames per second and the field of view is $600 \times 1200 \mu m^2$. All images shown in the article are extracted from videos taken with this framerate. Image processing and analysis were performed using mainly “Reslice”, “Measure” and “Analyse particles” functions of the ImageJ software.

C. Observations and results

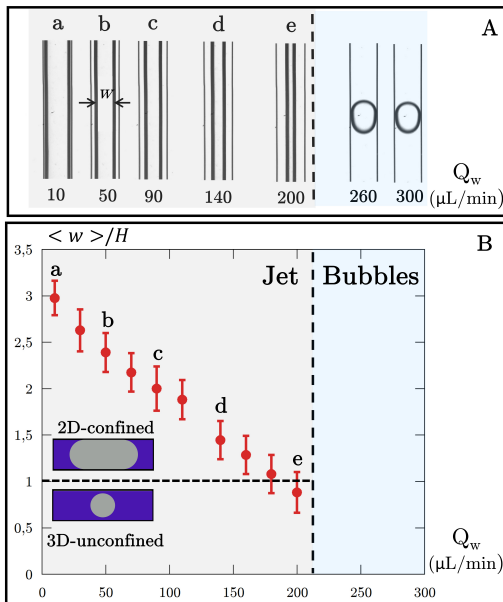


FIG. 3. A) Images of the two-phase flow observed for $\Delta P = 300$ mbar and different values of Q_w for the system without butanol. The vertical dashed line separates the domains for which a gas stream or gas bubbles are observed. B) Variation of the ratio between the gas jet mean width $\langle w \rangle$ and H as a function of Q_w . Insets of B: sketches of 2D-confined and 3D-unconfined jets represented in a vertical cross-section of the rectangular channel. The horizontal dashed line corresponds to the transition from a 2D-confined to a 3D-unconfined jet.

For the two liquid systems (without and with butanol), we work at a constant ΔP value in the range [100–300] mbar while increasing Q_w from 10 to 300 $\mu L/min$. Fig. 3A shows the evolution of the two-phase flow as a function of Q_w with no butanol. For low values of Q_w , we observe a stable jet whose uniform width, w , continuously decreases with Q_w (see Fig. 3B) until it becomes comparable to H where the jet, which is now 3D-unconfined, takes a cylindrical shape. As this shape is unstable with respect to the surface tension driven Rayleigh-Plateau instability, the jet then breaks and

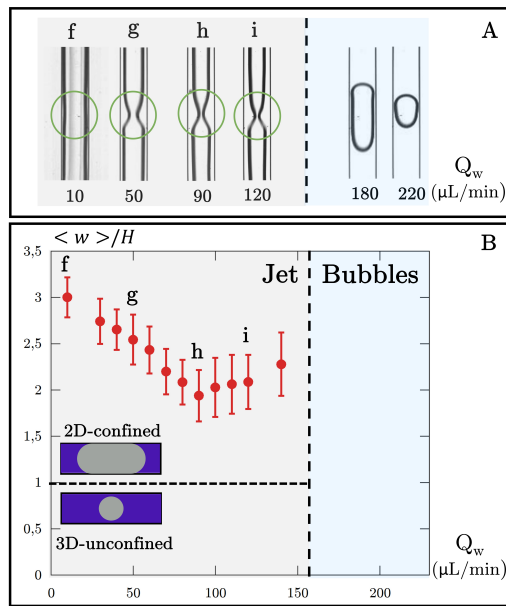


FIG. 4. A) Images of the two-phase flow observed for $\Delta P = 300$ mbar and different values of Q_w for the system with butanol. The green circles locate necks that spread without deforming. Multimedia views of images g and f are available. B) Variation of the ratio between the width of the gas jet $\langle w \rangle$ and H as a function of Q_w . Insets of B: sketches of 2D-confined and 3D-unconfined jets represented in a vertical cross-section of the rectangular channel. The horizontal dashed line corresponds to the transition from a 2D-confined to a 3D-unconfined jet.

forms monodisperse bubbles that are periodically emitted in a dripping regime (Fig. 3A). Such a behavior has been reported by Dollet¹ on a different gas/liquid surfactant system.

Very surprisingly, when butanol is added to the liquid phase, the behaviour and the stability of the gas jet drastically differ, as displayed in Fig. 4A. For small values of Q_w , a gas jet still forms, however, its width is no longer uniform along the channel as some localized narrow necks are clearly noticeable (see multimedia views of images g and f). The gas jet mean width, $\langle w \rangle$ (this value is obtained by averaging over time the width of the jet at a fixed position along the microchannel), varies with Q_w (Fig. 4B) up to a critical flow rate value, above which the non-uniform jet breaks into monodisperse bubbles, although it is still globally 2D-confined.

To get a better understanding of the mechanism of destabilization of the gas stream phenomenon, we next study the width of a short neck as it is convected. As shown in Fig. 5, the amplitude of the disturbance δw , measured at different x positions along the main channel, increases until it reaches a steady state whose value depends on Q_w , as reported in Fig. 6. Surprisingly, we note that for $Q_w > 50$, the disturbed jet does not break into bubbles even though w_{min} is smaller than H and the jet therefore adopts a circular cross-section, locally.

In this steady state regime, the neck propagates at a constant velocity (Fig. 7A) while maintaining its shape (see multimedia views of images g and f). Interestingly, this non-linear thickness disturbance, localized in space and time, bears some sim-

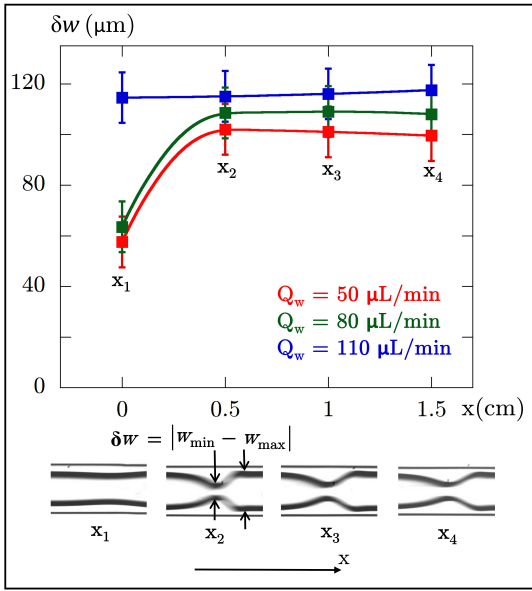


FIG. 5. Evolution of the amplitude of a neck, $\delta w = w_{max} - w_{min}$ that is observed for the system with butanol as a function of x (in cm), the channel position, for different values of Q_w . Insets: Images of the necks observed at different x for $Q_w = 50 \mu L/min$ and $\Delta P = 300 mbar$. Lines are only guide for the eyes.

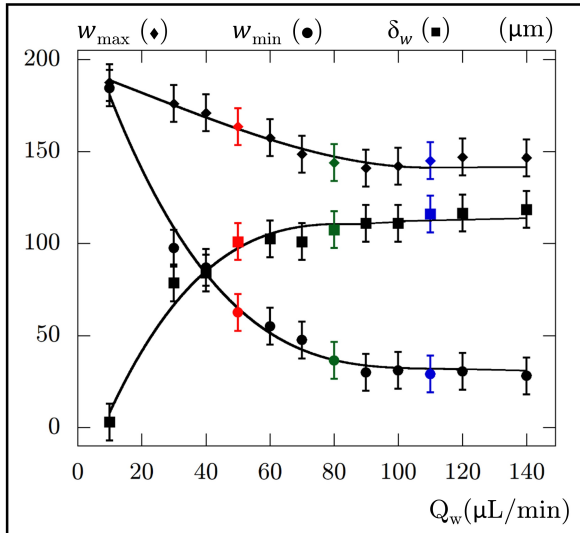


FIG. 6. Variation of the steady state values of w_{min} (\bullet), w_{max} (\blacklozenge) and $\delta w = w_{max} - w_{min}$ (\blacksquare) with Q_w when $\Delta P = 300 mbar$, for the butanol system. The values of these parameters (defined in Fig. 5) which characterize the neck geometry are measured at $x = 1 cm$. The values of Q_w for the symbols in red, green and blue are, as in Fig. 5, respectively 50, 80 and 110 $\mu L/min$. Lines are only guide for the eyes.

ilarities with a soliton. The formation of these necks occurs periodically and results from the growth of a small perturbation of the jet width that takes place near the cross-junction where the gas and the two liquid streams meet, very shortly after the laminar gas stream has been formed. Their mean production rate increases with Q_w (see Fig. 8). The propaga-

tion velocity of these necks also increases with Q_w and, in our experiments conducted at $\Delta P = 300 mbar$, it varies from 0.5 to 1.5 $m.s^{-1}$. It is also very important to outline that all the phenomena reported herein are not triggered by the evaporation of butanol, as experimentally, we observe no difference whether the gas used for our experiments is or is not saturated with butanol. As evidenced in Fig. 7B, the hydrodynamic instability that destabilizes the gas microfluidic stream develops in a very short time, the order of magnitude of which is the millisecond.

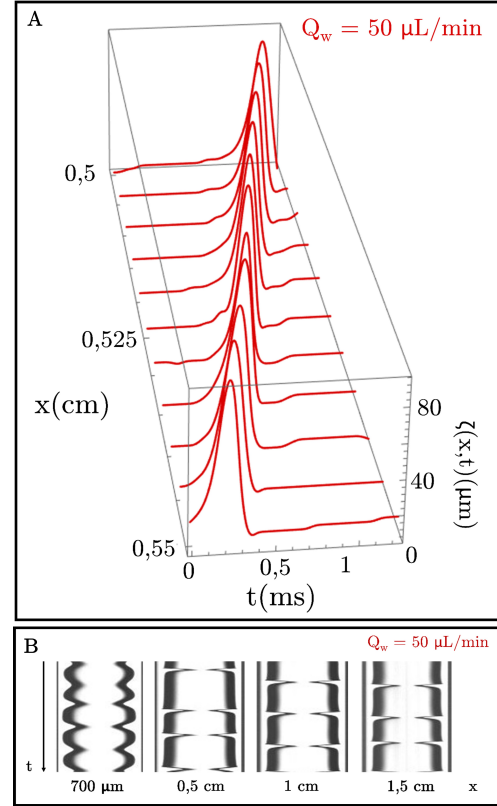


FIG. 7. A) The thickness profile of the liquid film, $\zeta = \frac{(W-w)}{2}$, along the x direction, is plotted at different times, t . The experimental variables are $\Delta P = 300 mbar$ and $Q_w = 50 \mu L/min$. B) Temporal variation of the jet width at four different x positions taken along the channel for $\Delta P = 300 mbar$ and $Q_w = 50 \mu L/min$.

III. THEORY:

A. A first qualitative explanation

To model the instability leading to the destabilization of the 2D-confined jet, it is first important to understand the effect of interfacial tension on the liquid pressure. Let us first consider the standard case, for which no Marangoni effects are considered (e.g. for which the surface tension remains constant). In a cylindrical 3D-unconfined geometry, any variation of the radius R of a gas thread having a constant pressure, P_0 , leads to two contributions for the

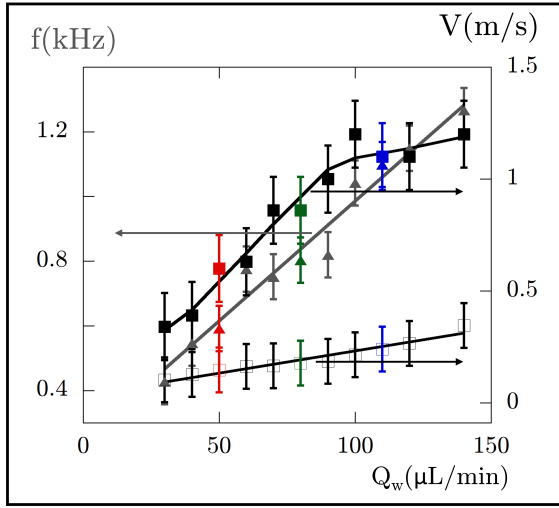


FIG. 8. Variations of the mean production rate, f (\blacktriangle), and velocity (\blacksquare), of the steady state necks with Q_w when $\Delta P=300$ mbar. Evolution of the fluid mean velocity, V_w (\square) with Q_w when $\Delta P=300$ mbar. The values of Q_w (given in $\mu\text{L}/\text{min}$) for the symbols in red, green and blue are, as in Fig. 5, respectively 50, 80 and 110. Lines are only guide for the eyes.

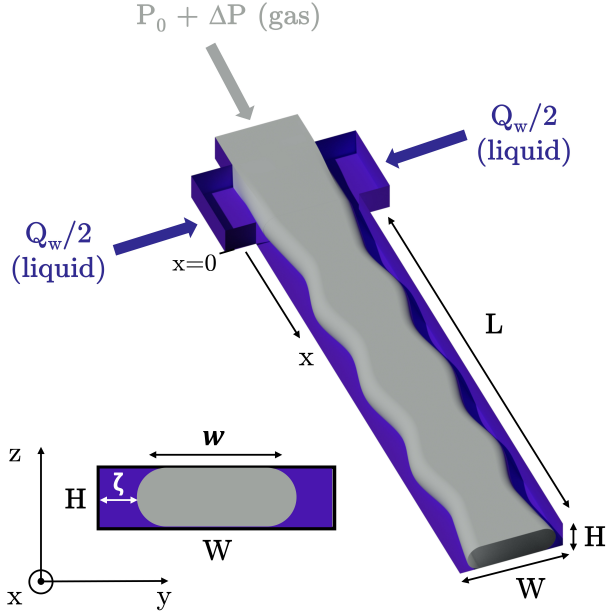


FIG. 9. Sketch of the cross-section of a $2D$ -confined gas stream in a vertical plane. Schematic representation of a $2D$ -confined gas stream for which the disturbance of the fluid thickness taken at half-height of the channel varies periodically along the flow direction x , according to $\zeta(x)=\bar{\zeta}+\delta\zeta e^{ikx}$.

Laplace pressure because of the two curvatures that characterize the gas-liquid interface. These contributions, which write $-\gamma/R(x)$ and $\gamma\frac{\partial^2 R(x)}{\partial x^2}$ with γ the gas/liquid surface tension, are respectively related to the curvature normal to the interface and to that along the x -axis. The first one is responsible for the Rayleigh-Plateau instability as for a radius disturbance

of the complex form, $R(x,t)=\bar{R}+\delta R e^{ikx}$, the pressure disturbance in the liquid writes in a linear approximation : $\delta P_l=\gamma(\frac{1}{\bar{R}^2}-k^2)\delta R e^{ikx}$ (\bar{R} and k are respectively the value of the radius of the unperturbed jet and the wavevector of the radius disturbance). The system is then always unstable since for $k\bar{R}<1$, the liquid pressure is larger in the liquid regions where $R(x,t)>\bar{R}$ than in the regions where $R(x,t)<\bar{R}$ so that a liquid flow results leading to an increase of the amplitude of the disturbance, δR . The gas stream is then unstable and breaks into gas bubbles.

For a $2D$ -confined jet, the situation is however different as the cross section of the jet is, to a good approximation, a rectangle of dimensions $(w-H)\times H$ bounded with two half circles of radius $H/2$, as illustrated in Fig. 9. Such an approximation holds because the capillary numbers at play in our experiments, $Ca=\eta V/\gamma\ll 1$ and because the gas does not wet the PDMS surface¹. One of the two curvature radii of the interface is therefore constant and equal to $H/2$ so that the Laplace pressure contribution now writes:

$$P_L = -\gamma\frac{2}{H} + \gamma\frac{\partial^2 w/2}{\partial x^2} \quad (1)$$

where w is the width of the jet.

When γ is constant, for a disturbance of the form $w(x,t)=\bar{w}+\delta w e^{ikx}$, the pressure disturbance in the liquid writes in a linear approximation : $\delta P_l=-\gamma k^2\delta w e^{ikx}$ (\bar{w} and k are respectively the width of the unperturbed jet and the wavevector of the width disturbance). The system is therefore always stable as for any k value, the liquid pressure is larger in the regions where $w(x,t)<\bar{w}$ than in the regions where $w(x,t)>\bar{w}$. As a result of this liquid pressure gradient, a flow of liquid from the former regions to the latter ones occurs and leads to a decrease of the amplitude of the disturbance, δw that hence always stabilizes the system.

The simple Rayleigh-Plateau picture depicted above well rationalizes our observations made on the Tween 20 surfactant system with no butanol for which the gas stream becomes unstable only when it becomes $3D$ -unconfined (i.e. with a circular cross-section, as depicted in inset of Fig. 4B). However, it fails to explain why, for the system with butanol, the gas stream may destabilize although it is still $2D$ -confined and therefore should be stable.

Interestingly, maximum bubble pressure measurements reveal that the total adsorption of butanol molecules on the gas/liquid interface occurs faster than 10 ms (the resolution of this apparatus for such a solution) in contrast to the Tween 20 surfactant molecules of our systems. The destabilization of the $2D$ -confined gas microfluidic stream, which occurs on a millisecond time scale, may therefore result from Marangoni effects as butanol molecules may have time to partially adsorb onto the gas/liquid interface. The Marangoni effect is responsible for froth in liquid mixtures⁴⁵. The interface of a liquid mixture is always enriched by the molecules exhibiting the lowest surface tension (butanol here) as compared to the bulk. Under surface extension, the surface concentration evolves and leads to an increase of γ , the surface tension. The

system after extension retrieves its thermodynamic equilibrium, through an exchange of molecules between the bulk and the interface and the value of γ becomes again equals to $\bar{\gamma}$. Along this line, a disturbance of the complex form $w(x,t)=\bar{w}+\delta w e^{ikx}$, generates an excess surface that modifies the local surface area fraction of the butanol molecules and hence leads to a disturbance of the local surface tension that in the linear regime takes the complex form $\gamma(x,t)=\bar{\gamma}+\delta\gamma e^{ikx}$. From Eq.(1), it therefore follows that the pressure liquid disturbance computed in the linear regime has now two terms as it is given by $\delta P_\ell=(\delta\gamma\frac{2}{H}-\bar{\gamma}k^2\delta w)e^{ikx}$. The second term is always stabilizing whereas the first term may possibly become destabilizing if the real part of the complex amplitude, $\delta\gamma$, is positive. A full analysis of the problem is not straightforward as it requires to theoretically describe the kinetics of adsorption of the butanol molecules on the disturbed interface. As this phenomenon involves an advection flux, it necessitate to compute the fluid velocity that strongly depends on the boundary Marangoni condition set by the adsorption of the butanol molecules⁴⁶. In the next paragraph, we detail this approach.

B. Modelling of the instability of a 2D-confined gas stream.

To check this plausible scenario, we perform a linear analysis of the stability of a thin layer of liquid of constant thickness, $\bar{\zeta}$, by considering a thickness disturbance of the form $\zeta(x,t)=\bar{\zeta}+\delta\zeta e^{ikx+st}$ and assuming that at the millisecond time scale of our microfluidic experiments, only the butanol molecules have time to adsorb at the gas/liquid interface (the Tween 20 molecules hence do not play any role for the destabilization phenomenon that we experimentally witness). In the linear regime, the surface concentration of the butanol molecules at the gas liquid interface writes $\Gamma(x,t)=\bar{\Gamma}+\delta\Gamma e^{ikx+st}$ so that the local surface tension varies accordingly to $\gamma(x,t)=\bar{\gamma}+\delta\gamma e^{ikx+st}$ where $\bar{\gamma}$ is the value of the gas/liquid surface tension for a butanol surface concentration equal to $\bar{\Gamma}$ that of the gas/liquid interface for the unperturbed liquid layer. Although evaporation may induce Marangoni effects⁴⁷⁻⁴⁹, we do not consider in our model the transfer by evaporation of the butanol molecules from the liquid to the gas. This simplification is justified, as we have experimentally checked that the destabilization of the 2D-confined gas jet is not triggered by the evaporation of butanol. Since the exchange of butanol molecules between the bulk and the interface is rather complex to theoretically describe, we decide to make the following three simplifying assumptions. Firstly, we consider that the adsorption/desorption kinetics of the butanol molecules at the interface from the bulk is mono-exponential, with a characteristic time, τ . Such an approximation which corresponds to a first order kinetics of adsorption is expected for a Langmuir model. We therefore consider that the butanol mass transfer mechanism is kinetically controlled and not diffusion controlled⁵⁰⁻⁵². Such assumption seems justified as the weight fraction of butanol in the bulk, 7 %, is quite large. Secondly, at the gas/liquid interface, we neglect the surface diffusive flow in front of the advective flow. This assumption is valid as long as the Peclet number at play which

is the inverse ratio between these two fluxes satisfies the following condition: $P_e=V\lambda/D\gg 1$ (V , λ and D are the fluid velocity at the gas/liquid interface, the wavelength of the surface disturbance and the surface diffusion coefficient of the butanol molecules (that we estimate to be similar to the bulk one), respectively^{46,53}. For our experiments this condition is well satisfied as $V\simeq 1\text{ ms}^{-1}$ and $\lambda\simeq 10^{-3}\text{ m}^{-1}$ (see Fig. 8) and $D\simeq 2,5\cdot 10^{-10}\text{ s}^{54}$, leading to Peclet numbers of the order of 10^7 . Thirdly, we consider that the surface tension of the water/butanol mixture obeys the Eberhart's equation⁵⁵ so that: $\gamma(\Gamma)=\Gamma\gamma_w+(1-\Gamma)\gamma_{but}$ where γ_w and γ_{but} are respectively the surface tension of water and of butanol with N_2 . With these ingredients, the kinetic evolution of Γ is given by⁴⁶:

$$\frac{\partial\Gamma}{\partial t}+\nabla_s\cdot(\mathbf{v}_{int}\Gamma)=\frac{\bar{\Gamma}-\Gamma}{\tau} \quad (2)$$

where \mathbf{v}_{int} is the fluid velocity vector at the gas/liquid interface) and where $\nabla_s=(\mathbf{I}-nn)\cdot\nabla$ and $(\mathbf{I}-nn)$ are respectively the surface gradient operator and the surface identity tensor, (n is the normal to the gas/liquid interface pointing towards the gas). The second term of the left hand side represents the advective flux of butanol at the interface. To determine \mathbf{v}_{int} , one must analytically solve the fluid flow within the cell. This is a difficult task because of the rectangular channel geometry, so we describe the physics of the problem by approximating the 3D velocity by a 2D one, at half-height of the channel. Although, such an approximation may seem severe as it necessitates that $(\frac{\zeta}{H})^2\ll 1$, it however permits to identify the physical origin of the instability that we witness as we will show below. Using a lubrication approximation (valid for $k\delta\zeta\ll 1$), we approximate the velocity field by a bidimensionnal one, oriented along the x direction, varying only in the (x,y) plane. Because of the no-slip condition at the wall and Marangoni effects, the velocity field within the liquid writes:

$$\mathbf{v}(x,y,t)=V(x,t)\frac{y[2\bar{\zeta}\zeta(x,t)-y+b(x,t)]}{\zeta(x,t)^2}\mathbf{e}_x \quad (3)$$

where $\frac{b(x,t)}{2}$ is the distance between the gas-liquid interface and the apex position of this parabolic profile (see Fig. 10). In the linear regime, $b(x,t)$ and $V(x,t)$ vary accordingly to $\bar{b}+\delta b e^{ikx+st}$ and $\bar{V}+\delta V e^{ikx+st}$, respectively. Note that: (i) \bar{V} is the liquid velocity at the gas/liquid interface if the thickness of the liquid layer is constant and (ii) $\bar{b}=0$ (for the unperturbed state, there is no Marangoni effect as the butanol surface concentration at the gas/liquid interface is constant). For the perturbed state, the fluid velocity vector at the gas/liquid interface, \mathbf{v}_{int} , is $\mathbf{v}(x,\zeta,t)=V_{int}(x,t)\mathbf{e}_x$ where:

$$V_{int}(x,t)=V(x,t)[1+b(x,t)/\zeta(x,t)] \quad (4)$$

With the lubrication approximation, Eq.(2) simplifies to:

$$\frac{\partial\Gamma}{\partial t}+\frac{\partial}{\partial x}(V_{int}\Gamma)=\frac{\bar{\Gamma}-\Gamma}{\tau} \quad (5)$$

By using Eberhart's equation, and Eq.(5), it is straightforward to derive that the kinetic equation that monitors the evolution

of $\gamma(x, t)$ writes:

$$\frac{\partial \gamma}{\partial t} + V_{int} \frac{\partial \gamma}{\partial x} = \frac{\bar{\gamma} - \gamma}{\tau} + E_g \bar{\gamma} \frac{\partial V_{int}}{\partial x} \quad (6)$$

where E_g is the dimensionless Gibbs elasticity modulus given by $E_g = \frac{\bar{\gamma} - \gamma}{\bar{\gamma}}$.

Because of the great viscosity difference between air and the liquid, the contribution of the gas to the interface stress is negligible compared to that of the liquid; so that the tangential stress balance at the gas-liquid interface writes:

$$\eta \frac{bV}{\bar{\zeta}^2} - \frac{\partial \gamma}{\partial x} = 0 \quad (7)$$

Writing the Navier-Stokes equation within the lubrication approximation and the above expression of the velocity field, yields the following equation:

$$2\eta \frac{V}{\bar{\zeta}^2} + \frac{\partial P}{\partial x} = 0 \quad (8)$$

where the pressure P in the liquid is the sum of the Laplace pressure $P_L = -\frac{2\gamma}{H} - \gamma \frac{\partial^2 \zeta}{\partial x^2}$ given in Eq.(1) and the pressure of the gas.

We close the problem by writing the volume conservation of the liquid:

$$\frac{\partial \zeta}{\partial t} + \frac{\partial Q}{\partial x} = 0 \quad (9)$$

where the flux $Q = \int_0^{\zeta(x,t)} v(x, y) dy = bV/2 + 2V\zeta/3$.

We perform a linear stability analysis on the set of equations 6, 7, 8, and 9 that monitors the spatio-temporal response of the system (e.g. of the disturbances δV , $\delta \zeta$, $\delta \gamma$ and δb that are proportional to e^{ikx+st} with k and s complex numbers that represent the wavevector and the growth rate of the fluctuations, respectively).

Because of the great viscosity difference between air and the liquid, the amplitude of the gas pressure perturbation is negligible compared to that of the liquid¹, with this convention, arranging the first order term of Eq.(8), using Eq.(1), leads to the following equation:

$$2\eta \frac{\bar{\zeta} \delta V - 2\bar{V} \delta \zeta}{\bar{\zeta}^3} + ik(k^2 \bar{\gamma} \delta \zeta - 2 \frac{\delta \gamma}{H}) = 0 \quad (10)$$

The conservation of the liquid volume yields at first order to:

$$s \delta \zeta + ik \left(\frac{2}{3} (\bar{\zeta} \delta V + \bar{V} \delta \zeta) + \frac{\bar{V} \delta b}{2} \right) = 0 \quad (11)$$

The stress continuity at the interface writes:

$$\eta \bar{V} \frac{\delta b}{\bar{\zeta}^2} - ik \delta \gamma = 0 \quad (12)$$

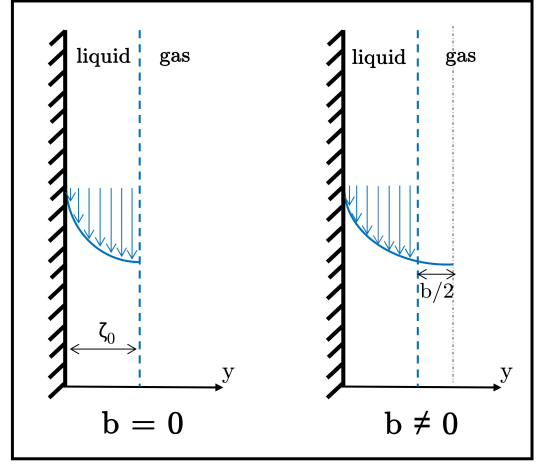


FIG. 10. Schematic representation of the parabolic velocity profile for the cases where $b=0$ and where $b \neq 0$. In the former case, there is no surface tension gradient at the interface and therefore no Marangoni effects.

Developing Eq.(4) at first order and using Eq.(6) gives the last equation:

$$-iE_g k \bar{\gamma} (\delta V + \frac{\bar{V} \delta b}{\bar{\zeta}}) + \delta \gamma (i\bar{V}k + s + \frac{1}{\tau}) = 0 \quad (13)$$

Eqs.(10-13) are a set of four linear equations for the four variables of the problem. The matrix of this linear system writes:

$$\begin{vmatrix} \frac{2\eta}{\bar{\zeta}^2} & 0 & ik^3 \bar{\gamma} - 4 \frac{\eta \bar{V}}{\bar{\zeta}^3} & -\frac{2ik}{H} \\ \frac{2ik\bar{\zeta}}{3} & \frac{ik\bar{V}}{2} & s + \frac{2ik\bar{V}}{3} & 0 \\ 0 & \frac{\bar{V}\eta}{\bar{\zeta}^2} & 0 & -ik \\ -iE_g k \bar{\gamma} & -\frac{ikE_g \bar{V} \bar{\gamma}}{\bar{\zeta}} & 0 & s + ik\bar{V} + \frac{1}{\tau} \end{vmatrix} \quad (14)$$

An instability appears if there is an eigen-mode for which s has a positive real part. A quick analysis of the problem reveals four dimensionless physical parameters, listed here: a capillary number, defined as $C_a = \eta \bar{V} / \bar{\gamma}$, another number $C_m = \frac{H\eta}{\bar{\gamma}\tau}$ that is the ratio of the water/butanol migration velocity H/τ to the capillary velocity, the ratio of the film thickness to the channel height, $X = \bar{\zeta}/H$, and E_g . We next introduce $q = k\bar{\zeta}$ and $S = s\tau$, the dimensionless wave-vector and growth rate of the fluctuation, respectively. By cancelling the determinant of the matrix given in (14), we then obtain a second order polynomial equation for S , shown below:

$$\begin{aligned} & -24C_a^2 q^2 + 4S(9iC_a C_m X q + \\ & C_m^2 X^2 + 3C_m E_g q^2 X(X+1) + C_m X q^4) + \\ & 4iC_a(6C_m X q + E_g q^3(2X+3) + q^5) + \\ & 12C_m^2 X^2 S^2 + 4C_m X q^4 + E_g q^6 = 0 \end{aligned} \quad (15)$$

By solving this dispersion equation using Mathematica, we extract two roots for $S(q)$ and hence $s(q)$. In the case where E_g vanishes, the two analytical solutions are:

$$s_1 = -\frac{1}{\tau} - ik\bar{V} \quad (16a)$$

and

$$s_2 = -\frac{k^4 \bar{\gamma} \bar{\zeta}^3}{3\eta} - 2ik\bar{V}\eta \quad (16b)$$

They correspond to surfactant density waves and capillary waves, two fluctuation modes that are both damped and convected.

In Fig. 11, we plot, $R_e(S)$, the real part of $S(q)$, for these two modes as a function of q for an illustrative case where Marangoni effects take place (i.e., $E_g \neq 0$) and another case with no Marangoni effects (i.e., $E_g = 0$). As expected, when $E_g = 0$, these two modes are always stable as $R_e(S) < 0$ for all q values. However, when $E_g \neq 0$, our model very interestingly demonstrates that one of the two modes becomes unstable as it exhibits a q domain where $R_e(S) > 0$ whereas the other mode remains stable. Four dimensionless numbers are at play in our problem. To investigate the influence of (\bar{V}) and $\bar{\zeta}$ on the stability of the liquid layer for a given liquid system, we numerically establish a stability diagram in the $[\log(C_a), X]$ plane, where we report domains where the system is stable (i.e., $R_e(S) < 0$) and unstable (i.e., $R_e(S) > 0$), the values of $C_m = \frac{H\eta}{\bar{\gamma}\tau}$ and E_g being kept constant as they only depend on the physico-chemical properties of the gas/fluid system considered (η , $\bar{\gamma}$, τ and E_g) and of H . In Fig. 12, we report such stability diagrams established for four different values of E_g and the same value of C_m . Our numerical results show that for $E_g = 0$ (for which there is no Marangoni effects), the liquid layer is always stable whatever the flow conditions. When $E_g \neq 0$, for any X value, the system becomes unstable when the capillary number is large enough. These diagrams show that as the value of E_g increases, the unstable region becomes wider on the stability diagrams.

C. Results and discussion

In our microfluidic experiments, the destabilization of the gas/liquid interface occurs on a millisecond time scale (see Fig. 7B). On such a short timescale, for our liquid systems, Tween 20 molecules do not have time to adsorb on this interface. For the system with no butanol, the value of the surface tension $\bar{\gamma}$ at this gas/liquid interface is therefore constant and roughly equal to that of water $\gamma_w = 72.4 \text{ mN.m}^{-1}$. Any disturbance of this gas/liquid surface therefore does not generate Marangoni effects as the surface coverage by Tween 20 surfactant molecules (and hence the value of γ , the surface tension) is not able to vary significantly during such a short time. We therefore conclude that Marangoni effects induced by the sole adsorption of Tween 20 surfactant molecules are unable to destabilize the 2D-confined microfluidic jet for our

surfactant system with no butanol. Experimentally, this is exactly what we observe as the gas stream becomes unstable and forms bubbles only when it becomes 3D-unconfined.

For the system with butanol, the physical situation is very different as the butanol molecules may now have time to adsorb on the gas liquid interface since their adsorption time is very short (as revealed with the maximum bubble pressure tensiometer: at 10 ms, the adsorption of the butanol molecules is quasi-total). Unfortunately because of the time resolution of the maximum bubble pressure apparatus, we have no experimental means to characterize the adsorption of the butanol molecules on the gas/liquid interface (and henceforth the gaz/liquid surface tension) for times shorter than 10 ms. Because of these experimental limitations, we can only qualitatively compare our model predictions to our experimental findings as the values of $\bar{\gamma}$, E_g and τ are impossible to determine exactly. Experimentally, we can just state that $\tau \leq 10^{-2} \text{ s}$. Under the fast extension of the gas/liquid surface induced by a disturbance, as the newly created surface is populated by the molecules present in the bulk, its composition is that of the bulk. Using a cuboid approximation and the Eberhart's approximation⁵⁵ for computing the surface tension, the value of the dynamic surface tension at $t=0 \text{ s}$ is estimated to $\gamma_0 = 70.9 \text{ mN.m}^{-1}$. As $\gamma_0 > \bar{\gamma} \geq \gamma_{but}$ it therefore follows that $0 < E_g \leq 1.8$.

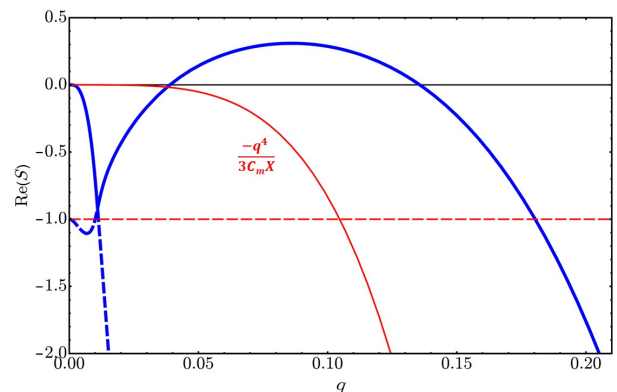


FIG. 11. $R_e(S)$ of the two fluctuation modes as a function of q for a system with and without Marangoni effects for which the values of E_g are respectively 0.2 (blue curves) and 0 (red curves). For both systems $C_a = 8.10^{-3}$, $C_m = 1.10^{-4}$ and $X = 0.4$. The dashed and continuous lines correspond to surfactant density waves and capillary waves, respectively.

In Fig. 12, we indicate in the $[\log(C_a), X]$ plane, the domains where the system is stable (i.e., $R_e(S) < 0$) and unstable (i.e. $R_e(S) > 0$), for a fixed value of $C_m = 4.6 \cdot 10^{-4}$ (which corresponds to $\tau = 6 \cdot 10^{-3} \text{ s}$) and four different values of E_g . Very interestingly, we note that for $E_g = 0$ the jet is always stable whereas it may become unstable when the value of E_g is different from zero. The diagram obtained for $E_g = 1.8$ show an excellent agreement between theoretical predictions and our experimental observations while respecting $\tau \leq 10^{-2} \text{ s}$ and $0 < E_g \leq 1.8$.

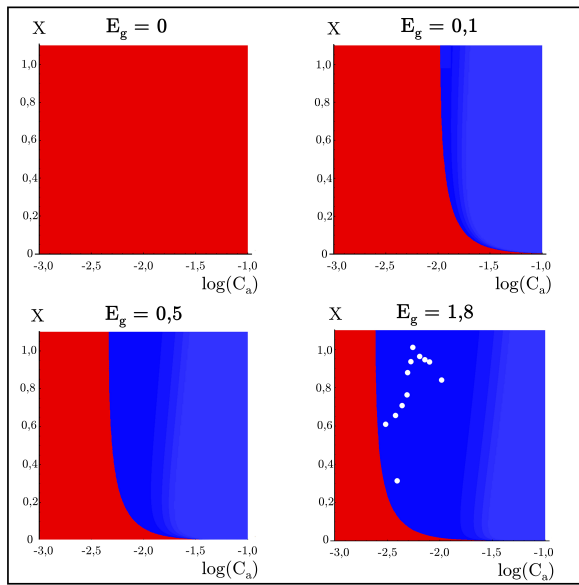


FIG. 12. Stability diagrams in the $[\log(C_a), X]$ plane, numerically computed with $C_m = 4.6 \cdot 10^{-4}$ (which corresponds to $\tau = 6 \cdot 10^{-3}$ s) and 4 different E_g . The blue (resp. red) areas correspond to unstable (resp. stable) regions. In the last diagram, the white circles correspond to the experimental conditions of our experiments conducted at $\Delta P = 300$ mbar, for all Q_w value in the jet regime (i.e. between 10 and $140 \mu\text{L}/\text{min}$) (see Fig.4).

IV. CONCLUSION:

In closing, despite its simplicity, our model seems to well corroborate our experimental observations. We therefore believe that we have identified the key ingredients at play in the destabilization of $2D$ -confined microfluidic gas streams. This phenomenon only occurs when the adsorption time of the chemical species promoting such effects is of the order of the characteristic time of the microfluidic flow, that is typically $\simeq 1\text{ms}$. Experimentally, we have shown that the addition of a few % of butanol in the surfactant solution phase permits to witness such effects. We anticipate that this experimental system may also lead to Marangoni effects on various physical phenomena such as droplet impacts, splashes to name a few⁵⁶ for which the characteristic hydrodynamic timescales at play are also very short.

ACKNOWLEDGMENTS

This work was funded by a CIFRE Fellowship (2020-1424) from TotalEnergies S.E. We thank A. Saint-Jalmes for his help for surface tension measurements and A. Colin and B. Dollet for fruitful discussions.

¹B. Dollet, W. van Hoeve, J. Raven, P. Marmottant, and M. Verluis, "Role of the channel geometry on the bubble pinch-off in flow-focusing," *Phys. Rev. Lett.* **100**(3), 034504 (2008).

²P. Guillot, A. Colin, and A. Ajdari, "Stability of a jet in confined pressure-driven biphasic flows at low reynolds number in various geometries," *Phys. Rev. E* **78**(1), 016307 (2008).

- ³L. Salkin, A. Schmit, P. Panizza, and L. Courbin, "Making soap bubbles by blowing air onto a soap film," *Phys. Rev. Lett.* **116**(7), 077801 (2016).
- ⁴L. Tan, W. Zhu, and K. Zhou, "Recent progress on polymer materials for additive manufacturing," *Adv. Funct. Mater.* **30**(43), 2003062 (2020).
- ⁵S. Lin and R. Reitz, "Drop and spray formation from a liquid jet," *Annu. Rev. Fluid Mech.* **30**, 85–105 (1998).
- ⁶J. Lasheras and E. Hopfinger, "Liquid jet instability and atomization in a co-axial gas stream," *Annu. Rev. Fluid Mech.* **32**, 275 (2000).
- ⁷R. Ruo, F. Chen, C. Chang, and M. Chang, "Three-dimensional response of unrelaxed tension to instability of viscoelastic jets," *J. Fluid Mech.* **682**, 558–576 (2011).
- ⁸E. Antonopoulou, O. Harlen, M. Rump, T. Segers, and M. Walkley, "Effect of surfactants on jet break-up in drop-on-demand inkjet printing," *Phys. Fluids* **33**(7), 072112 (2021).
- ⁹H. Grace, "Monodisperse fragmentation in emulsions :mechanisms and kinetics," *Europhys. Lett.* **61**(5), 708–714 (2003).
- ¹⁰C. Mabilbe, F. Leal-Calderon, J. Bibette, and V. Schmitt, "Monodisperse fragmentation in emulsions :mechanisms and kinetics," *Europhys. Lett.*, volume =.
- ¹¹W. Drenckhan and A. Saint-Jalmes, "The science of foaming," *Adv. Colloid Interface Sci.* **222**, 228–259 (2015).
- ¹²J. Montanero and A. Ganan-Calvo, "Dripping, jetting and tip streaming," *Rep. Prog. Phys.* **83**(9), 097001 (2020).
- ¹³J. Plateau, *Statique expérimentale et théorique des liquides soumis aux seules forces moléculaires* (Gauthier-Villars:Paris, France, 1873).
- ¹⁴L. Rayleigh, "On the capillary phenomena of jets," *Proc. R. Soc. London.* **29**, 71–97 (1879).
- ¹⁵K. Humphry, A. Ajdari, A. Fernandez-Nieves, H. Stone, and D. Weitz, "Suppression of instabilities in multiphase flow by geometric confinement," *Phys. Rev. E* **79**(5), 056310 (2009).
- ¹⁶W. Engl, K. Ohata, P. Guillot, A. Colin, and P. Panizza, "Selection of two-phase flow patterns at a simple junction in microfluidic devices," *Phys. Rev. Lett.* **96**(13), 134505 (2006).
- ¹⁷P. Guillot, A. Colin, A. Utada, and A. Ajdari, "Stability of a jet in confined pressure-driven biphasic flows at low reynold numbers," *Phys. Rev. Lett.* **99**(10), 104502 (2007).
- ¹⁸A. Utada, A. Fernandez-Nieves, H. Stone, D. Weitz, A. Utada, and A. Ajdari, "Dripping to jetting transitions in coflowing streams," *Phys. Rev. Lett.* **99**(9), 094502 (2007).
- ¹⁹A. Utada, A. Fernandez-Nieves, H. Stone, D. Weitz, A. Utada, and A. Ajdari, "Absolute instability of a liquid jet in a coflowing stream," *Phys. Rev. Lett.* **100**(1), 014502 (2008).
- ²⁰G. Cabezas, M. Herrada, and M. Montanero, "Stability of a jet moving in a rectangular microchannel," *Phys. Rev. E* **100**(5), 053104 (2019).
- ²¹S. Vagner, S. Patlazhan, C. Serra, D. Funfschilling, and V. Kulichikhin, "Dripping and jetting of semi-dilute polymer solutions in co-axial capillaries," *Phys. Fluids* **33**(6), 062002 (2021).
- ²²K. Mu, R. Qiao, T. Si, X. Cheng, and H. Dinh, "Interfacial instability and transition of jetting and dripping modes in a co-flow focusing process," *Phys. Fluids* **33**(5), 052118 (2021).
- ²³S. Anna, N. Bontoux, and H. Stone, "Formation of dispersions using flow focusing in microchannels," *Appl. Phys. Lett.* **82**(3), 364 (2003).
- ²⁴P. Garstecki, H. Stone, and G. Whitesides, "Mechanism for flow-rate controlled breakup in confined geometries: a route to monodisperse emulsions," *Phys. Rev. Lett.* **94**(16), 164501 (2005).
- ²⁵W. Engl, R. Backov, and P. Panizza, "Controlled production of emulsions and particles by milli and microfluidic techniques," *Curr. Opin. Colloid Interface Sci.* **13**(4), 206–216 (2008).
- ²⁶P. Zhu and L. Wang, "Passive active droplet generation with microfluidics: a review," *Lab Chip* **17**(11), 34–75 (2017).
- ²⁷T. Cubaud, M. Tatineni, X. Zhong, and C. Ho, "Bubble dispenser in microfluidic devices," *Phys. Rev. E* **72**(3), 037302 (2005).
- ²⁸P. Garstecki, M. Fuerstman, H. Stone, and G. Whitesides, "Formation of droplets and bubbles in a microfluidic t-junction-scaling and mechanism of break-up," *Lab Chip* **6**(5), 437–446 (2006).
- ²⁹W. van Hoeve, B. Dollet, J. Gordillo, M. Verluis, L. van Wijngaarden, and D. Lohse, "Bubble size prediction in coflowing streams," *Eur. Phys. Lett.* **94**(6), 64001 (2011).
- ³⁰S. Anna, "Droplets and bubbles in microfluidic devices," *Annu. Rev. Fluid Mech.* **48**, 285–309 (2016).

- ³¹M. Mein, C. L. Men, K. Loubière, G. Hebrard, and N. Dietrich, “Taylor bubble formation and flowing in a straight millifluidic channel with a cross inlet: Part i bubble,” *Chem. Eng. Sci.* **255**, 117609 (2022).
- ³²C. Cramer, P. Fisher, and E. Windhab, “Drop formation in a co-flowing ambient fluid,” *Chem. Eng. Sci.* **59**, 3045–3058 (2004).
- ³³H. Liu and Y. Zhang, “Droplet formation in microfluidic cross-junction,” *Phys. Fluids* **23(8)**, 082101 (2011).
- ³⁴L. Ngo, S. Joo, and C. Byon, “Effects of junction angle and viscosity ratio on droplet formation in microfluidic cross-junctions,” *J Fluids Eng.* **138**, 051202 (2016).
- ³⁵W. Yu, X. Liu, Y. Zhao, and Y. Chen, “Droplet generation hydrodynamics in the microfluidic cross-junction with different junction angles,” *Chem. Eng. Sci.* **203**, 259–284 (2019).
- ³⁶T. Dinh and T. Cubaud, “Role of the interfacial tension on viscous multiphase flows in coaxial microfluidic channels,” *Langmuir* **37(2)**, 7420–7429 (2021).
- ³⁷T. Cubaud, B. Conry, X. Hu, and T. Dinh, “Diffusive and capillary instabilities of viscous fluids threads in microchannels,” *Phys. Rev. Fluids* **6(9)**, 094202 (2021).
- ³⁸Z. Liu, Y. Ma, X. Wang, Y. Pang, Y. Ren, and D. Li, “Experimental and theoretical studies on neck thinning dynamics of droplets in cross junctions microchannels,” *Exp. Therm. Fluid Sci.* **139**, 110739 (2022).
- ³⁹M. de Saint Vincent, H. Chraïbi, and J. Delville, “Optical flow focusing: light-induced destabilization of a stable liquid thread,” *Phys. Rev. App.* **4(4)**, 044005 (2015).
- ⁴⁰P. Cheng, D. Li, L. Boruvka, Y. Rotenberg, and A. Neuman, “Automation of axisymmetric drop shape analysis for measurement of interfacial tensions and contact angles,” *Colloid Surf. A* **43**, 151–167 (1990).
- ⁴¹R. Bendure, “Dynamic surface tension determination with the maximum bubble pressure method,” *J. Colloid Interface Sci.* **35(2)**, 238–248 (1971).
- ⁴²V. Fainerman, V. Kazakov, S. Lylyk, and A. M. R. Miller, “Dynamic surface tension measurements of surfactant solutions using the maximum bubble pressure method – limits of applicability,” *Colloid Surf. A* **250**, 97–102 (2004).
- ⁴³V. Fainerman, V. Mys, A. Makievski, J. Petkovc, and R. Miller, “Dynamic surface tension of micellar solutions in the millisecond and submillisecond time range,” *J. Colloid Interface Sci.* **302(1)**, 40–46 (2006).
- ⁴⁴D. Duffy, J. McDonald, O. Schueller, and G. Whitesides, “Rapid prototyping of microfluidic systems in poly(dimethylsiloxane),” *Anal. Chem.* **70(23)**, 4974–4984 (1998).
- ⁴⁵H. P. Tran, M. Arangalage, L. Jorgensen, N. Passade-Boupat, F. Lequeux, and L. Talini, “Understanding frothing of liquid mixtures: a surfactant effect at the origin of enhanced liquid film lifetimes,” *Phys. Rev. Lett.* **125(17)**, 178002 (2020).
- ⁴⁶H. Manikantan and T. Squires, “Surfactant dynamics: hidden variables controlling fluid flows,” *J. Fluid Mech.* **892**, P1 (2020).
- ⁴⁷F. Wodlei, J. Sebilliau, J. Magnaudet, and V. Pimienta, “Marangoni-driven flower-like patterning of an evaporating drop spreading on a liquid substrate,” *Nat. Commun.* **9(1)**, 820 (2018).
- ⁴⁸R. Nazareth, G. Karapetsas, K. Sefiane, O. Matar, and P. Valluri, “The stability of slowly evaporating thin liquid films of binary mixtures,” *Phys. Rev. Fluid* **5(10)**, 104007 (2020).
- ⁴⁹H. Liu and J. Deng, “Influence of marangoni effects on heat and mass transfer during evaporation of sessile microdroplets,” *Micromachines* **13**, 1968 (2022).
- ⁵⁰F. Jin, R. Balasubramaniam, and K. J. Stebe, “Surfactant adsorption to spherical particles: the intrinsic length scale governing the shift from diffusion to kinetic-controlled mass transfer,” *J. Adhes.* **80**, 773–796 (2004).
- ⁵¹Q. Brosseau, J. Vrignon, and J. C. Baret, “Microfluidic dynamic interfacial tensiometry (μ dit),” *Soft Matter* **10(17)**, 3066–3076 (2014).
- ⁵²F. He, P. Yazhgur, A. Salonen, and D. Langevin, “Adsorption-desorption kinetics of surfactants at liquid interfaces,” *Adv. Colloid Interface Sci.* **222**, 377–384 (2015).
- ⁵³T. Bickel, “Spreading dynamics of reactive surfactants driven by marangoni convection,” *Soft Matter* **15(18)**, 3644–3648 (2019).
- ⁵⁴T. Cubaud, B. Conry, X. Hu, and T. Dinh, “Swelling of diffusive fluid threads in microchannels,” *Phys. Rev. Lett.* **125(17)**, 174502 (2020).
- ⁵⁵J. G. Eberhart, “The surface tension of binary liquid mixtures,” *J. Phys. Chem.* **70(4)**, 1183–1186 (1966).
- ⁵⁶G. Gillot, J. Gemeaux, L. Simon, and L. Benyahia, “Fast dynamics of surfactant probed by the acoustic of drop impact,” *Phys. Fluids* **34(7)**, 072107 (2022).